

Diverse Image Harmonization

Xinhao Tao, Tianyuan Qiu, Junyan Cao, Li Niu*
 MoE Key Lab of Artificial Intelligence, Shanghai Jiao Tong University
 {taoxinhao, frank.qiu, joy_c1, ustcnewly}@sjtu.edu.cn

Abstract

Image harmonization aims to adjust the foreground illumination in a composite image to make it harmonious. The existing harmonization methods can only produce one deterministic result for a composite image, ignoring that a composite image could have multiple plausible harmonization results due to multiple plausible reflectances. In this work, we first propose a reflectance-guided harmonization network, which can achieve better performance with the guidance of ground-truth foreground reflectance. Then, we also design a diverse reflectance generation network to predict multiple plausible foreground reflectances, leading to multiple plausible harmonization results. The extensive experiments on the benchmark datasets demonstrate the effectiveness of our method.

1. Introduction

Image composition [33] refers to combining visual elements from different images into a realistic composite image, which has diverse applications from everyday photo editing to automatic advertising. To tackle the illumination discrepancy between foreground and background, image harmonization aims to adjust the illumination of foreground to produce a harmonious image. Specifically, given a composite image I_c and foreground mask M , image harmonization model produces a harmonization result. Recently, deep learning based image harmonization has made huge progress. The existing methods formulate image harmonization as image translation [7, 14, 19, 37] or color transformation [8, 12, 26, 45], producing visually pleasant results.

All the above methods can only produce one deterministic result for a composite image. However, a composite image may actually have multiple plausible harmonization results. According to the Retinex theory [22], an image I could be decomposed into reflectance map A and illumination map L : $I = A * L$, in which $*$ means element-wise

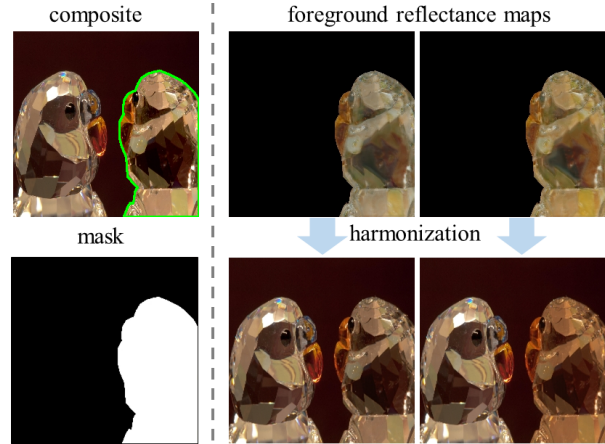


Figure 1. An example of multiple plausible harmonization results when the foreground reflectance is uncertain.

product. Intuitively, the reflectance map represents the essential color and the illumination map represents the environmental lighting. Given the foreground in composite image I_c , it is sometimes difficult to determine its reflectance and there could be multiple plausible reflectances. Therefore, **when transferring the background illumination to the foreground, different foreground reflectances would yield different harmonization results**, which is referred to as diverse image harmonization in this paper. We provide one example of diverse image harmonization in Figure 1. The composite foreground is a yellow glass figurine. It is hard to determine whether it is a white figurine under yellow illumination or a yellow figurine under white illumination. The harmonization results for these two cases should be different.

One way to disambiguate the foreground reflectance is referring to the original foreground image I_o that the foreground belongs to. **Compared with the foreground, I_o contains richer colors and semantics, which could help determine the illumination and thus further determine the foreground reflectance.** In the most commonly used harmonization dataset iHarmony4 [7], the composite images are synthetic, so there are no real I_o , but we can

*Corresponding author.

approximately acquire I_o (see Section 3.1). In the real composite image datasets like RealHM [19], we naturally have the original foreground images I_o . With I_o , we can use neural rendering model [47] to extract the ground-truth foreground reflectance map A_{gt} , because it matches the foreground reflectance in the ground-truth harmonized image. We observe that with the ground-truth foreground reflectance as auxiliary input, the reflectance-guided harmonization network could better predict the ground-truth harmonization result.

In practice, we may not have I_o and thus A_{gt} is unavailable. To address this issue, we design a novel diverse reflectance generation network solely based on the foreground. Specifically, the network takes in a foreground and a random vector, producing multiple plausible foreground reflectances A_{pre} by sampling random vectors. By using different A_{pre} as the auxiliary input of harmonization network, we can obtain multiple plausible harmonization results. Extensive experiments demonstrate that our reflectance generation network can generate diverse and reasonable A_{pre} , and the reflectance-guided harmonization network can produce multiple plausible harmonization results which are consistent with the variation of A_{pre} .

In summary, our major contributions can be summarized as follows,

- We explore diverse image harmonization considering uncertain foreground reflectance.
- We propose a reflectance-guided harmonization network, which reveals that ground-truth foreground reflectance can help approach ground-truth harmonized result.
- We design a diverse reflectance generation network to produce diverse and reasonable foreground reflectances, leading to multiple reasonable harmonization results.

2. Related Works

2.1. Image Harmonization

Image harmonization can be broadly categorized into traditional methods and deep learning based methods. Traditional image harmonization methods [24, 34, 38, 46, 49] primarily focus on designing color transformations to match the visual appearance between foreground and background. Deep learning based approaches [2, 4, 5, 9, 13, 15–17, 19, 27, 35, 36, 39, 40, 44] have become mainstream in the field of image harmonization. DoveNet [7] introduced the first large-scale iHarmony4 dataset. IIH [14] decomposed composite images into reflectance and illumination components, and performed self-supervised training. iS²AM [37] proposed the integration of S²AM [9] module to better capture the relation between the background and foreground. Recently, CDTNet [8], DCCF [45], PCT-Net [12], and other methods [21, 26, 30, 43] utilized deep learning networks to predict transformation coefficients, achieving further en-

hancement in performance while efficiently scaling to high-resolution images.

However, all the above harmonization methods assume that the harmonization result is deterministic, which is problematic. Our method is the first to generate multiple plausible harmonization results given a composite image.

2.2. Diverse Image-to-Image Translation

Diverse image-to-image translation aims to transform an input image in the source domain to multiple possible outputs in the target domain. We focus on supervised diverse image-to-image translation, which provides one ground-truth output for each input image. For example, BicycleGAN [50] combined cVAE-GAN [18, 23, 25] and cLRGAN [6, 10, 11], allowing the generation of multiple plausible results for a single input image while also mitigating the mode collapse problem. PixelNN [1] employed the nearest-neighbor method to combine pixel matching, thereby converting incomplete conditional inputs into multiple outputs. Subsequently, many studies have been done for the diverse image generation tasks. For example, PiiGAN [3] used an additional style extractor. PUT [29] utilized a patch-based vector quantized variational auto-encoder [41] and an unquantized transformer. PICNet [48] refined cVAE [23] to fit the inpainting task, while ICT [42] improved generative performance through Gibbs sampling and transformers.

In our task, we have one ground-truth harmonization result for a composite image, but there could be multiple plausible results, which falls into the scope of supervised diverse image-to-image translation. We are the first to explore diverse image harmonization.

3. Our Method

Given a composite image I_c and foreground mask M , our goal is generating multiple plausible harmonization results. According to Retinex theory [22], an image I can be decomposed into reflectance map A and illumination map L : $I = A * L$, where $*$ is element-wise product. In a composite image, the foreground reflectance map is independent of the background and estimable based on the foreground region. Solely based on the foreground region, the foreground reflectance map could have multiple possibilities, and different foreground reflectance maps would lead to different harmonization results.

If we have the foreground reflectance map matching the ground-truth harmonized foreground, which is referred to as ground-truth foreground reflectance map A_{gt} , we expect it could help produce the harmonization result closer to the ground-truth. Therefore, we adapt the existing harmonization network to accept the foreground reflectance map as an auxiliary input, guiding the generation of harmonization results. We will introduce how to extract ground-truth foreground reflectance map in Section 3.1 and investigate the

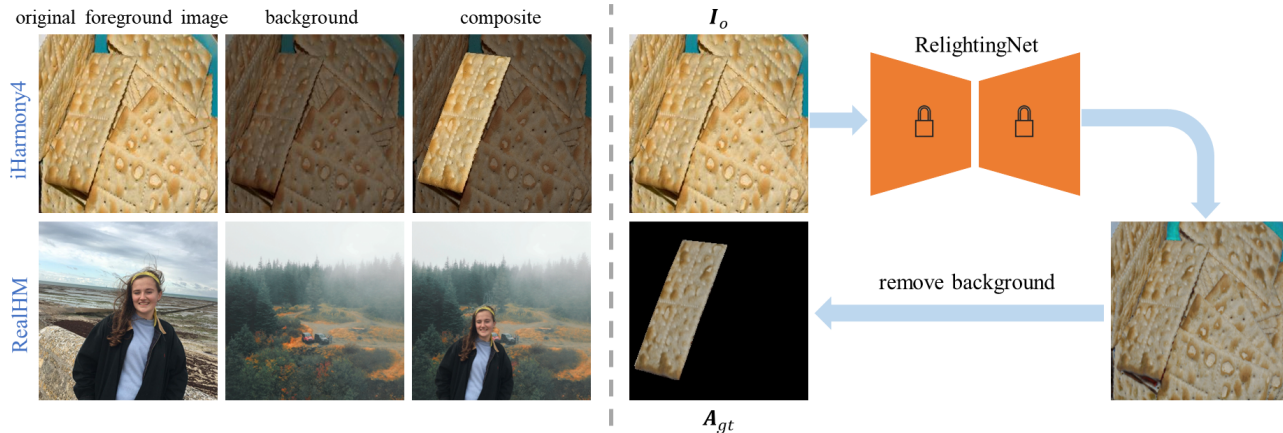


Figure 2. In the left part, we show two example triplets of original foreground image, background, and composite image on iHarmony4 [7] and RealHM [19]. In the right part, we use pretrained RelightingNet [47] to extract the ground-truth foreground reflectance map A_{gt} from the original foreground image I_o .

effectiveness of using ground-truth foreground reflectance map as guidance in Section 3.2. n.

In practice, the ground-truth foreground reflectance map A_{gt} is often unavailable, so we design a diverse reflectance generation network to produce multiple plausible foreground reflectance maps A_{pre} based on the composite foreground, which will be detailed in Section 3.3. Finally, the generated foreground reflectance maps can be fed into our reflectance-guided harmonization model to produce multiple plausible harmonization results.

3.1. Ground-truth Reflectance Extraction

When we only have the composite foreground, the illumination information is often ambiguous, and thus its foreground reflectance map is also ambiguous. However, if we possess the original foreground image I_o that the foreground belongs to, we can infer the overall illumination more easily based on I_o with complex semantics and colors, thereby determining the ground-truth foreground reflectance map A_{gt} . Next, we will discuss how to get I_o from the existing harmonization datasets.

The iHarmony4 [7] dataset is the most commonly used large-scale dataset for image harmonization, comprising four sub-datasets constructed in different ways. iHarmony4 is a synthetic dataset, in which the foregrounds of real images are adjusted to create synthetic composite images. Thus, there are no original foreground images that the composite foregrounds belong to. However, we can simulate the original foreground images I_o for experiments.

The four sub-datasets in iHarmony4 can be divided into two groups. The first group contains HCOCO and HFlickr, in which the composite foregrounds are adjusted from real foregrounds using traditional color transfer methods. We can apply the same color transfer to the entire real image

to simulate I_o . The second group contains HAdobe5k and Hday2night, in which each scene is associated with a set of images (captured over time or retouched by photographers). The foreground in one image I is superseded by that in another image I' to create a composite image I_c , so we can take I' as the original foreground image I_o . For all sub-datasets, simulated I_o are essentially obtained by making global illumination adjustments towards the ground-truth real image, so the foreground reflectance map in I_o matches that in the ground-truth image.

Besides the synthetic dataset, we also consider the real dataset RealHM [19] consisting of real composite images, in which the composite foregrounds are cropped from one image and pasted on another background image, so we naturally have the original foreground images I_o that composite foregrounds belong to. The ground-truth images in RealHM are obtained by manually adjusting the composite foregrounds. We conjecture that when manually adjusting the composite foregrounds, the original foreground images are observed to better estimate the foreground reflectance map. Thus, the foreground reflectance map in I_o matches that in ground-truth image.

In summary, for both synthetic dataset iHarmony4 and real dataset RealHM, we can get simulated or real original foreground images I_o , in which the foreground reflectance map matches that in ground-truth image. Then, we use off-the-shelf reflectance prediction model to extract the reflectance map from I_o . Specifically, we employ the inverse neural rendering model RelightingNet [47], which can decompose an image into a reflectance map and an illumination map. Although the results are not perfectly accurate, we observe that most predicted reflectance maps are reasonable. Figure 2 provides a detailed illustration of the various forms of I_o for different datasets and the process of getting

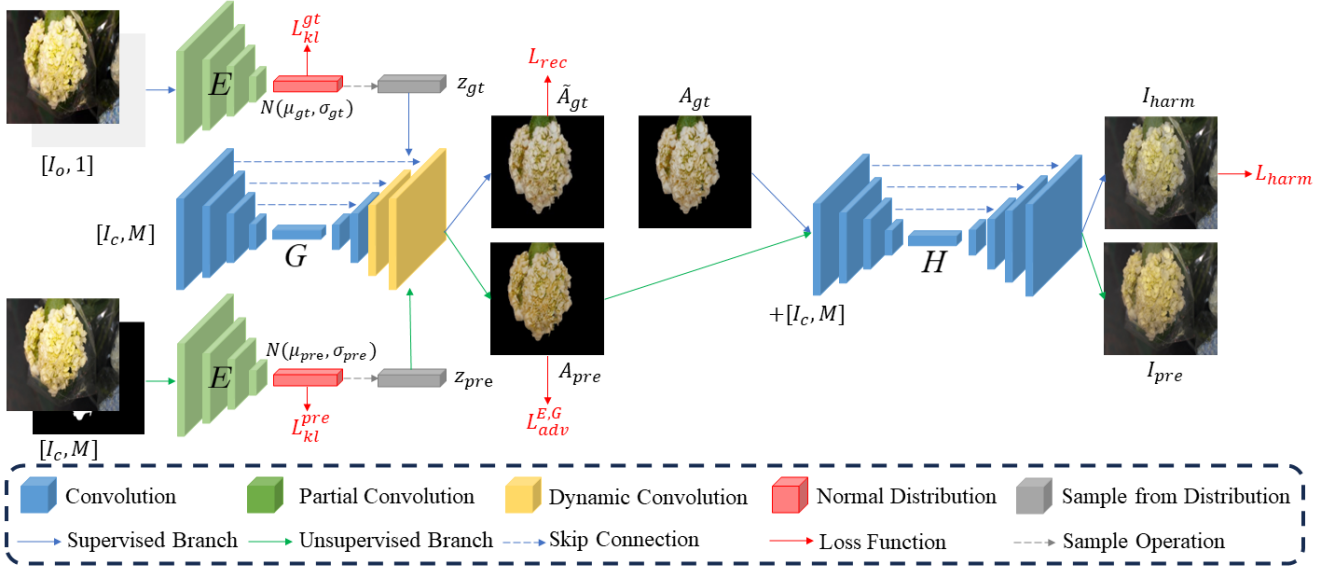


Figure 3. The left part shows the diverse reflectance generation network with two branches: supervised and unsupervised branch. In the supervised branch, we extract the guidance code from I_o , which guides the network G to reconstruct the ground-truth foreground reflectance map. In the unsupervised branch, we extract the guidance code from the foreground region, which guides G to predict plausible foreground reflectance maps. The right part shows the reflectance-guided harmonization network, in which foreground reflectance map is appended to the input to guide the harmonization process.

A_{gt} , which will be used in Section 3.2 and 3.3.

3.2. Reflectance-Guided Image Harmonization

We conjecture that provided with ground-truth foreground reflectance map A_{gt} , the uncertainty of harmonization process could be alleviated, and the harmonization result should be closer to the ground-truth image. In other words, the ground-truth foreground reflectance maps could serve as auxiliary information for arbitrary harmonization network to improve the performance.

Considering that the existing image harmonization methods have quite diverse network structures, we opt for the simplest strategy to inject ground-truth foreground reflectance map into network without severely distorting the network structure. Specifically, we concatenate A_{gt} with the original input $[I_c, M]$ channel-wisely, which is sent to the harmonization network to produce the harmonized image I_{harm} . Different harmonization methods also have different loss functions. For simplicity, we opt to maintain the original loss function for each method, which is denoted as L_{harm} .

3.3. Diverse Reflectance Generation

However, in practical applications, we usually do not have access to the original foreground image I_o and thus cannot get A_{gt} . In this case, we only have the composite foreground and its foreground reflectance map is uncertain. Therefore, we aim to generate multiple reasonable fore-

ground reflectance maps for the composite foreground. To reach this goal, we design a novel diverse reflectance generation network with two branches: supervised branch and unsupervised branches. Both branches share the reflectance generation U-Net, which takes in the composite foreground and a random vector to produce a foreground reflectance map. The random vector serves as the guidance code. We can get multiple foreground reflectance maps by sampling the guidance code multiple times. However, the distributions of guidance codes in two branches are different. In the supervised branch, the guidance code follows the encoded distribution from I_o . Under the guidance of I_o , the predicted foreground reflectance map is expected to approach A_{gt} . In the unsupervised branch, the guidance code follows the encoded distribution from I_c , making it usable at test time when I_o is unavailable. Next, we will introduce reflectance generation U-Net and the two branch separately.

3.3.1 Reflectance Generation U-Net

We adopt U-Net G in [37], which takes in composite foreground $[I_c, M]$ and predicts the foreground reflectance map. Various approaches have been explored in previous works to inject a guidance code z into the network. For more effective utilization of z , following [20], we use z to predict dynamic kernels, which act upon the decoder feature maps in the U-Net. Specifically, we first pass z through several fully connected layers to get w , which contains the

Backbone	Method	All			HCOCO			HFlickr			HAdobe5k			Hday2night		
		MSE	fMSE	PSNR	MSE	fMSE	PSNR	MSE	fMSE	PSNR	MSE	fMSE	PSNR	MSE	fMSE	PSNR
iS ² AM	base	24.64	262.67	37.95	16.48	266.14	39.16	69.68	443.63	33.56	22.59	166.19	37.24	40.59	591.07	37.72
	fg	25.45	277.68	38.03	17.70	285.08	38.94	70.83	457.96	33.48	21.62	163.08	38.06	54.81	778.49	36.85
	gt	21.37	231.01	38.59	14.62	240.61	39.49	54.90	344.73	34.42	20.75	148.60	38.47	39.87	552.47	37.79
	pred(10)	22.94	243.51	38.58	15.79	251.28	39.51	61.84	381.17	34.27	21.29	155.99	38.46	38.05	557.82	37.80
PCT-Net	base	18.16	216.25	39.85	10.72	208.26	40.78	44.30	341.10	35.13	21.25	157.24	39.97	44.74	654.81	37.65
	fg	22.11	261.06	38.95	13.25	257.87	39.88	56.62	401.92	34.36	24.87	184.64	38.97	48.15	728.09	37.48
	gt	16.93	199.41	39.92	10.62	198.14	40.76	40.46	279.18	35.76	19.06	144.63	40.00	38.98	633.27	37.68
	pred(10)	17.72	209.45	39.96	11.51	208.21	40.86	43.09	303.87	35.71	18.67	150.01	39.94	44.18	627.06	37.87

Table 1. Quantitative comparison on iHarmony4 dataset. The best results for each backbone network are denoted in boldface.

input channel weights of the dynamic convolution kernel. The convolution kernel modulated by w is applied to the final feature map in the decoder, and the resultant feature map accounts for predicting the foreground reflectance map. For the details of dynamic kernel, please refer to [20].

3.3.2 Supervised Branch

In the supervised branch, we have the original foreground image I_o . We aim to reconstruct the ground-truth foreground reflectance map A_{gt} under the guidance of I_o . We employ the encoder E to encode I_o into the Gaussian distribution $\mathcal{N}(\mu_{gt}, \sigma_{gt})$. Subsequently, we sample from this distribution to get the guidance code z_{gt} by using reparameterization trick [23]. To regulate the encoded distribution, we introduce a KL divergence loss to enforce $\mathcal{N}(\mu_{gt}, \sigma_{gt})$ to be close to unit Gaussian distribution:

$$L_{kl}^{gt} = KL[\mathcal{N}(\mu_{gt}, \sigma_{gt}) || \mathcal{N}(\mathbf{0}, \mathbf{1})]. \quad (1)$$

z_{gt} is injected into the reflectance generation U-Net to predict the foreground reflectance map \tilde{A}_{gt} , which is pushed towards A_{gt} . As we are only interested in the foreground region, we adopt a foreground MSE loss L_{rec} :

$$L_{rec} = \|\tilde{A}_{gt} * M - A_{gt}\|^2, \quad (2)$$

where $*$ means element-wise multiplication.

3.3.3 Unsupervised Branch

In the unsupervised branch, we cannot access the original foreground image I_o . Thus, we use the composite image $[I_c, M]$ to get the guidance code. First, we extend the encoder E by using partial convolutions [28] to extract information from partial image based on the provided mask M . For the supervised branch, we can use all-one mask, in which case partial convolution reduces to vanilla convolution. Similar to the supervised branch, We employ E to encode $[I_c, M]$ into the Gaussian distribution $\mathcal{N}(\mu_{pre}, \sigma_{pre})$, and sample the guidance code z_{pre} from

this distribution. Since $\mathcal{N}(\mu_{pre}, \sigma_{pre})$ should have certain overlap with $\mathcal{N}(\mu_{gt}, \sigma_{gt})$, we add a KL divergence loss to prevent that $\mathcal{N}(\mu_{pre}, \sigma_{pre})$ deviates too far from $\mathcal{N}(\mu_{gt}, \sigma_{gt})$:

$$L_{kl}^{pre} = KL[\mathcal{N}(\mu_{pre}, \sigma_{pre}) || \mathcal{N}(\mu_{gt}, \sigma_{gt})]. \quad (3)$$

Then, similar to the supervised branch, we sample the guidance code z_{pre} from $\mathcal{N}(\mu_{pre}, \sigma_{pre})$ and inject it into G to produce the foreground reflectance map A_{pre} . To ensure the effectiveness of the unsupervised branch, we adopt adversarial learning to make the predicted foreground reflectance maps indistinguishable from real foreground reflectance maps. Specifically, we utilize the discriminator in [32], denoted as D_a . The discriminator takes in the foreground information $[A_{pre}, I_c * M, M]$ and predicts the realism score, in which $I_c * M$ functions as the conditional information to help judge the realism of A_{pre} . Under the adversarial learning framework, we update the generator $\{E, G\}$ and the discriminator D_a alternately. When updating the generator $\{E, G\}$, we expect the produced A_{pre} to confuse the discriminator D_a . We adopt the least-square adversarial loss [31]:

$$L_{adv}^{E,G} = (D_a(A_{pre}, I_c * M, M) - 1)^2. \quad (4)$$

When training the discriminator D_a , we expect it to distinguish A_{pre} from real foreground reflectance maps. Hence, the loss function can be written as:

$$L_{adv}^{D_a} = (D_a(A_{gt}, I_c * M, M) - 1)^2 + D_a(A_{pre}, I_c * M, M)^2. \quad (5)$$

Combining two branches, the total loss function for training $\{E, G\}$ can be summarized as

$$L_{E,G} = L_{rec} + L_{kl}^{gt} + L_{kl}^{pre} + \lambda L_{adv}^{E,G}, \quad (6)$$

in which the hyper-parameter λ is set as 0.1 empirically.

During test time when the original foreground image is unavailable, we can use the unsupervised branch to produce multiple plausible foreground reflectance maps, which are delivered to the reflectance-guided harmonization network in Section 3.2 to generate multiple plausible harmonization results.



Figure 4. The harmonization results of iSSAM [37] and PCT-Net [12] on iHarmony4 dataset when using or without using ground-truth foreground reflectance map.

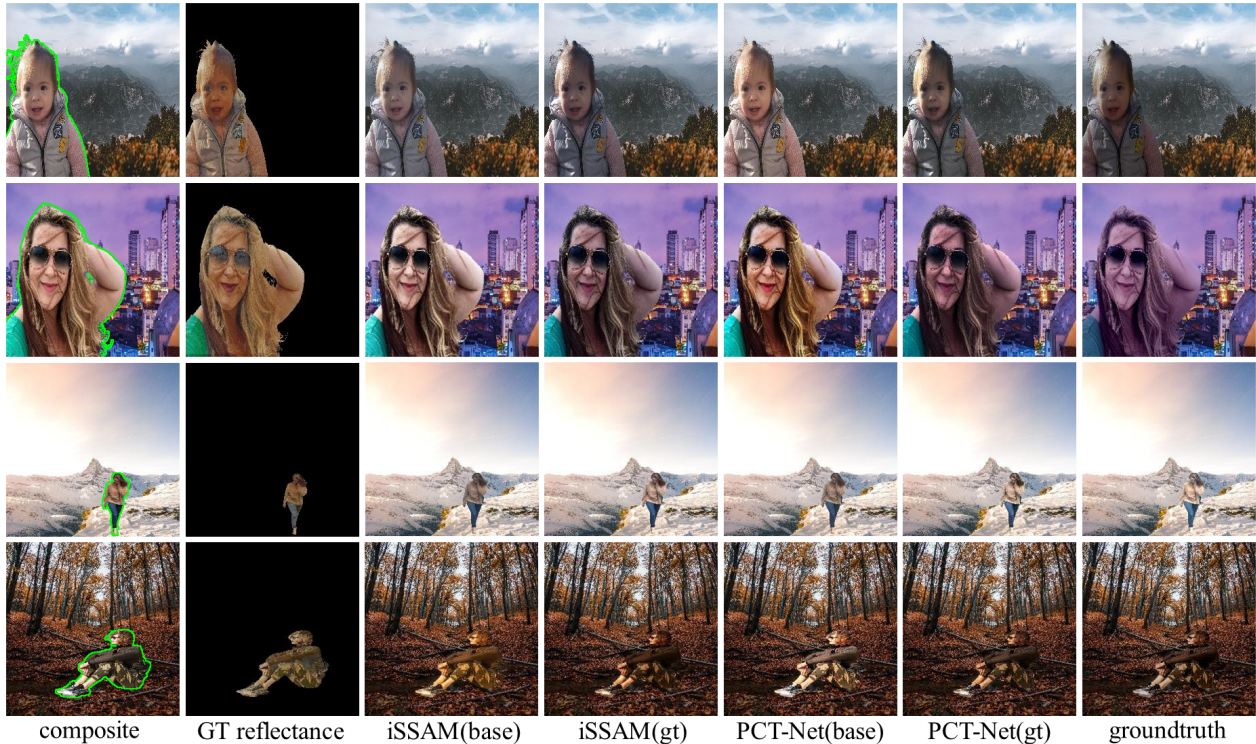


Figure 5. The harmonization results of iSSAM [37] and PCT-Net [12] on realHM dataset when using or without using ground-truth foreground reflectance map.

4. Experiments

4.1. Datasets and Implementation Details

We conduct experiments on the iHarmony4 dataset with four sub-datasets and the RealHM dataset. Because the RealHM dataset only contains 218 images, we utilize it solely for evaluation. As mentioned in Section 3.1, we can get the original foreground images I_o and the ground-truth foreground reflectance maps A_{gt} for these datasets.

Regarding the harmonization backbone network H , we employ iS^2AM and PCT-Net as two examples to show the effectiveness of ground-truth foreground reflectance maps in Section 4.2. As the overall performance of PCT-Net is superior to iS^2AM , we use PCT-Net by default in the remaining sections unless otherwise stated. Our experimental environment is Ubuntu 18.04, CUDA 11.3, four RTX-3090 GPUs with 24GB memory, and PyTorch 1.10 framework. In line with prior works, we adopted Mean Squared Error (MSE), foreground Mean Squared Error (fMSE), and Peak Signal-to-Noise Ratio (PSNR) as evaluation metrics.

4.2. Effectiveness of Ground-truth Reflectance

In this section, we compare the harmonization results of different backbone networks with or without the ground-truth foreground reflectance maps.

The quantitative outcomes are reported in Table 1. In “base” row, we report the results of the basic backbone network without using ground-truth foreground reflectance maps. In “gt” row, we report the results of our reflectance-guided harmonization network using ground-truth foreground reflectance maps. The comparison between the two rows shows that the integration of ground-truth foreground reflectance maps can make the harmonization results closer to the ground-truth.

Recall that we use the entire original foreground image to extract the ground-truth foreground reflectance map, because the complex colors and semantics of the entire original foreground image can help alleviate the illumination uncertainty. To validate this point, we extract the foreground reflectance map using only the foreground region and use it in our reflectance-guided harmonization network. The results are reported in “fg” row. We can see that the performances of “fg” are much worse than “gt”, and even worse than “base”, indicating that the extracted foreground reflectance map may not match the ground-truth and thus harms the harmonization performance.

The qualitative results on iHarmony4 are shown in Figure 4, from which we can see that including ground-truth foreground reflectance map makes the harmonization results more closely aligned with the ground-truth image.

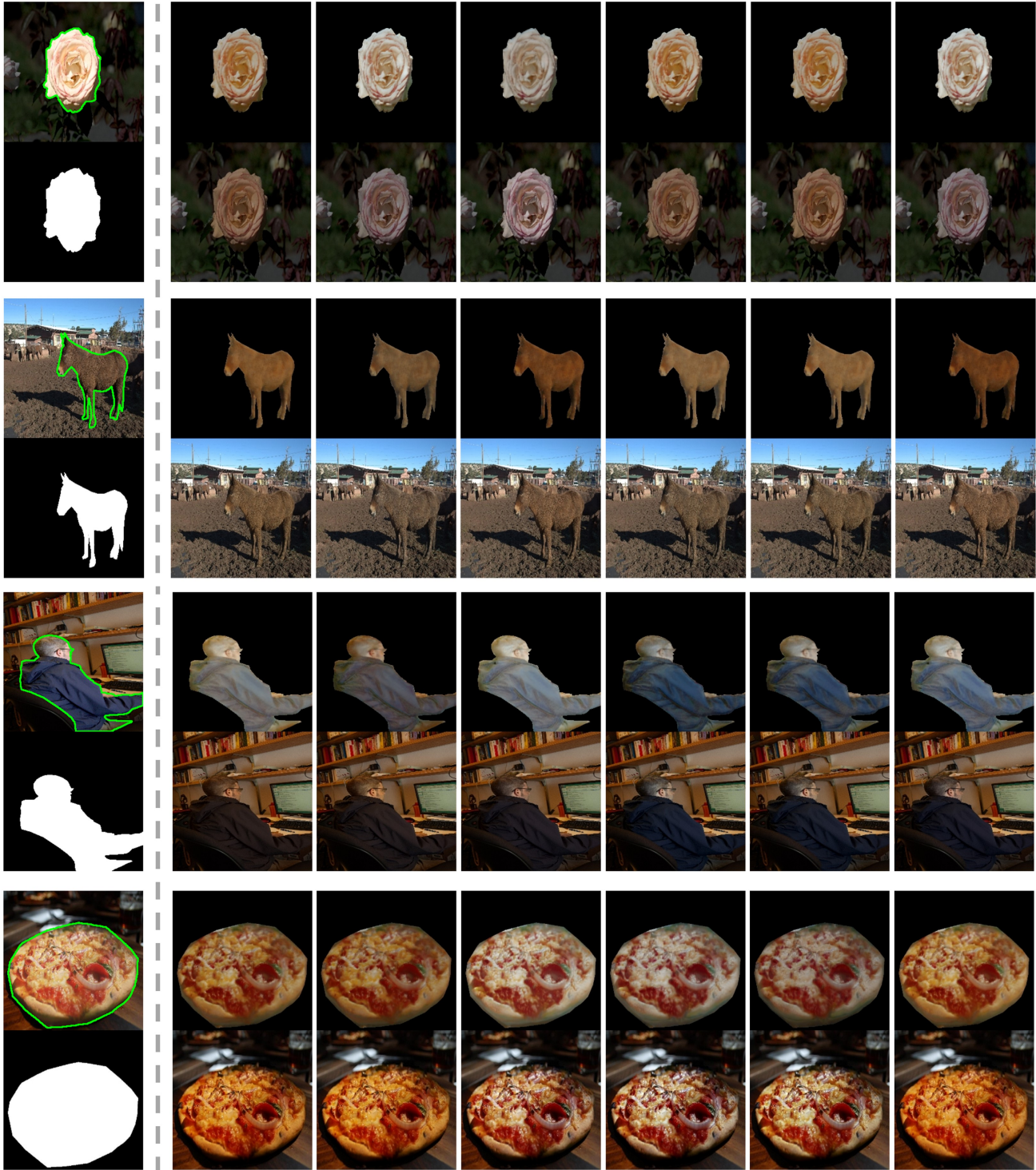


Figure 6. Illustration of multiple possible harmonization results arising from the reflectance uncertainty. In each example, the top row represents the predicted foreground reflectance maps, while the bottom row represents the corresponding harmonization result.

As analysed in Section 3.1, iHarmony4 is a synthetic dataset with simulated original foreground images. In contrast, RealHM contains real original foreground images. To

further verify the effectiveness of ground-truth foreground reflectance map in real-world cases, we report the results of “base” and “gt” on RealHM in Table 2. Since we train the

Backbone	Method	MSE ↓	fMSE ↓	PSNR ↑
iS ² AM	base	415.61	2004.07	25.31
	gt	294.89	1414.42	26.46
PCT-Net	base	385.57	1760.69	26.08
	gt	319.47	1493.79	26.36

Table 2. Quantitative comparison on RealHM dataset.

model on iHarmony4 and evaluate on RealHM, the overall results in Table 2 are much worse than those in Table 1, due to the huge domain gap between these two datasets. Nevertheless, the results in “gt” row significantly outperform those in “base” row, which again validates the effectiveness of ground-truth foreground reflectance map. We also provide qualitative results on RealHM in Figure 5. Although harmonization on RealHM is challenging, the incorporation of A_{gt} notably enhances the performance.

4.3. Diverse Harmonization Results

In this work, we target at diverse image harmonization. Thus, we show the diversity and plausibility of our approach by providing multiple generated foreground reflectance maps A_{pre} and the corresponding harmonization results in Figure 6. Specifically, we first use our diverse reflectance generation network (unsupervised branch) to generate multiple foreground reflectance maps A_{pre} . Then, we use A_{pre} in our reflectance-guided harmonization network to produce multiple harmonization results. In the first example, it is challenging to determine the hue (pure white or a little pinkish) and brightness of foreground illumination. Hence, there could be multiple plausible foreground reflectance maps. In the second example, although the horse’s color should be brown, its reflectance map could still vary due to the uncertain illumination brightness.

Furthermore, we can observe a trend of consistency between the harmonization results and the foreground reflectance maps, emphasizing the importance of foreground reflectance in the harmonization process. For instance, a darker reflectance corresponds to a darker harmonization result in both examples.

We also attempt to analyze the plausibility of multiple harmonization results quantitatively. In particular, for each composite image, we generate 10 harmonization results and choose the one closest to the ground-truth for metric calculation, leading to row “pred(10)” in Table 1. The results in row “pred(10)” are better than those in row “base” and “fg”, and even better than those in row “gt” in some cases, which proves that our diverse reflectance generation network can produce plausible foreground reflectance maps.

Row	Method	fMSE ↓	LPIPS ↑
1	w/o supervised branch	362.81	0.0462
2	w/o unsupervised branch	297.48	0.0832
3	w/o encoding $[I_c, M]$	264.52	0.0587
4	w/o adversarial training	259.13	0.1165
5	w/o dynamic conv	230.17	0.0874
6	full	200.69	0.1031

Table 3. Ablation studies on iHarmony4 dataset.

4.4. Ablation Studies on Our Reflectance Generation Network

We conduct ablation studies on our diverse reflectance generation network in terms of both plausibility and diversity of the generated foreground reflectance maps. Given a composite image, we sample 10 times to get 10 results. For plausibility, we calculate the minimum fMSE compared with the ground-truth one. For diversity, we compute the average of all pairwise LPIPS.

The results are presented in Table 3. In row 1, we remove the supervised branch and enforce the encoded distribution in the unsupervised branch to approach $\mathcal{N}(0, 1)$. The generated results are poor and have mode collapse issue. In row 2, we remove the unsupervised branch and sample the guidance code from $\mathcal{N}(0, 1)$ during testing, leading to a significant performance drop. To further analyze the unsupervised branch, we remove the guidance encoding and adversarial training in row 3 and 4 respectively. Guidance encoding enhances diversity and plausibility, while adversarial training primarily improves plausibility. Lastly, as an alternative way to utilize the guidance code, we directly append the guidance code to the input of G in row 5, which degrades the overall performance.

5. Conclusion

In this work, we have studied the uncertainty of harmonization results due to the uncertainty of foreground reflectance. We have designed a reflectance-guided harmonization network and a diverse reflectance generation network. We have demonstrated that the ground-truth foreground reflectance map can benefit the harmonization performance. We have also shown that our method can produce diverse and plausible harmonization results.

References

- [1] Aayush Bansal, Yaser Sheikh, and Deva Ramanan. Pix-eln: Example-based image synthesis. *arXiv preprint arXiv:1708.05349*, 2017. 2
- [2] Zhongyun Bao, Chengjiang Long, Gang Fu, Daquan Liu, Yuanzhen Li, Jiaming Wu, and Chunxia Xiao. Deep image-based illumination harmonization. In *CVPR*, 2022. 2

- [3] Weiwei Cai and Zhanguo Wei. Piigan: generative adversarial networks for pluralistic image inpainting. *IEEE Access*, 8, 2020. 2
- [4] Xun Cai, Qingjie Shi, Yanbo Gao, Shuai Li, Wei Hua, and Tian Xie. A structure-preserving and illumination-consistent cycle framework for image harmonization. *IEEE Transactions on Multimedia*, 2023. 2
- [5] Jianqi Chen, Yilan Zhang, Zhengxia Zou, Keyan Chen, and Zhenwei Shi. Dense pixel-to-pixel harmonization via continuous image representation. *arXiv preprint arXiv:2303.01681*, 2023. 2
- [6] Xi Chen, Yan Duan, Rein Houthoofd, John Schulman, Ilya Sutskever, and Pieter Abbeel. Infogan: Interpretable representation learning by information maximizing generative adversarial nets. *NIPS*, 2016. 2
- [7] Wenyan Cong, Jianfu Zhang, Li Niu, Liu Liu, Zhixin Ling, Weiyuan Li, and Liqing Zhang. Dovenet: Deep image harmonization via domain verification. In *CVPR*, 2020. 1, 2, 3
- [8] Wenyan Cong, Xinhao Tao, Li Niu, Jing Liang, Xuesong Gao, Qihao Sun, and Liqing Zhang. High-resolution image harmonization via collaborative dual transformations. In *CVPR*, 2022. 1, 2
- [9] Xiaodong Cun and Chi-Man Pun. Improving the harmony of the composite image by spatial-separated attention module. *IEEE Transactions on Image Processing*, 29:4759–4771, 2020. 2
- [10] Jeff Donahue, Philipp Krähenbühl, and Trevor Darrell. Adversarial feature learning. *arXiv preprint arXiv:1605.09782*, 2016. 2
- [11] Vincent Dumoulin, Ishmael Belghazi, Ben Poole, Olivier Mastropietro, Alex Lamb, Martin Arjovsky, and Aaron Courville. Adversarially learned inference. *arXiv preprint arXiv:1606.00704*, 2016. 2
- [12] Julian Jorge Andrade Guerreiro, Mitsuru Nakazawa, and Björn Stenger. Pct-net: Full resolution image harmonization using pixel-wise color transformations. In *CVPR*, 2023. 1, 2, 6, 7
- [13] Zonghui Guo, Dongsheng Guo, Haiyong Zheng, Zhaorui Gu, Bing Zheng, and Junyu Dong. Image harmonization with transformer. In *ICCV*, 2021. 2
- [14] Zonghui Guo, Haiyong Zheng, Yufeng Jiang, Zhaorui Gu, and Bing Zheng. Intrinsic image harmonization. In *CVPR*, 2021. 1, 2
- [15] Zonghui Guo, Zhaorui Gu, Bing Zheng, Junyu Dong, and Haiyong Zheng. Transformer for image harmonization and beyond. *IEEE Transactions on Pattern Analysis and Machine Intelligence*, 2022. 2
- [16] Yucheng Hang, Bin Xia, Wenming Yang, and Qingmin Liao. Scs-co: Self-consistent style contrastive learning for image harmonization. In *CVPR*, 2022.
- [17] Guoqing Hao, Satoshi Iizuka, and Kazuhiro Fukui. Image harmonization with attention-based deep feature modulation. In *BMVC*, 2020. 2
- [18] Geoffrey E Hinton and Ruslan R Salakhutdinov. Reducing the dimensionality of data with neural networks. *science*, 313(5786):504–507, 2006. 2
- [19] Yifan Jiang, He Zhang, Jianming Zhang, Yilin Wang, Zhe Lin, Kalyan Sunkavalli, Simon Chen, Sohrab Amirghodsi, Sarah Kong, and Zhangyang Wang. Ssh: A self-supervised framework for image harmonization, 2021. 1, 2, 3
- [20] Tero Karras, Samuli Laine, Miika Aittala, Janne Hellsten, Jaakko Lehtinen, and Timo Aila. Analyzing and improving the image quality of stylegan. In *CVPR*, 2020. 4, 5
- [21] Zhanghan Ke, Chunyi Sun, Lei Zhu, Ke Xu, and Rynson W.H. Lau. Harmonizer: Learning to perform white-box image and video harmonization. In *ECCV*, 2022. 2
- [22] Ron Kimmel, Michael Elad, Doron Shaked, Renato Keshet, and Irwin Sobel. A variational framework for retinex. *International Journal of computer vision*, 52(1):7–23, 2003. 1, 2
- [23] Diederik P Kingma and Max Welling. Auto-encoding variational bayes. *arXiv preprint arXiv:1312.6114*, 2013. 2, 5
- [24] Jean-François Lalonde and Alexei A. Efros. Using color compatibility for assessing image realism. In *ICCV*, 2007. 2
- [25] Anders Boesen Lindbo Larsen, Søren Kaae Sønderby, Hugo Larochelle, and Ole Winther. Autoencoding beyond pixels using a learned similarity metric. In *ICML*, 2016. 2
- [26] Jingtang Liang, Xiaodong Cun, Chi-Man Pun, and Jue Wang. Spatial-separated curve rendering network for efficient and high-resolution image harmonization. In *ECCV*, 2022. 1, 2
- [27] Jun Ling, Han Xue, Li Song, Rong Xie, and Xiao Gu. Region-aware adaptive instance normalization for image harmonization. In *CVPR*, 2021. 2
- [28] Guilin Liu, Fitsum A Reda, Kevin J Shih, Ting-Chun Wang, Andrew Tao, and Bryan Catanzaro. Image inpainting for irregular holes using partial convolutions. In *ECCV*, 2018. 5
- [29] Qiankun Liu, Zhentao Tan, Dongdong Chen, Qi Chu, Xiyang Dai, Yinpeng Chen, Mengchen Liu, Lu Yuan, and Nenghai Yu. Reduce information loss in transformers for pluralistic image inpainting. In *CVPR*, 2022. 2
- [30] Sheng Liu, Cong Phuoc Huynh, Cong Chen, Maxim Arap, and Raffay Hamid. Lemart: Label-efficient masked region transform for image harmonization. In *CVPR*, 2023. 2
- [31] Xudong Mao, Qing Li, Haoran Xie, Raymond YK Lau, Zhen Wang, and Stephen Paul Smolley. Least squares generative adversarial networks. In *ICCV*, 2017. 5
- [32] Mehdi Mirza and Simon Osindero. Conditional generative adversarial nets. *arXiv preprint arXiv:1411.1784*, 2014. 5
- [33] Li Niu, Wenyan Cong, Liu Liu, Yan Hong, Bo Zhang, Jing Liang, and Liqing Zhang. Making images real again: A comprehensive survey on deep image composition. *arXiv preprint arXiv:2106.14490*, 2021. 1
- [34] Erik Reinhard, Michael Ashikhmin, Bruce Gooch, and Peter Shirley. Color transfer between images. *IEEE Computer Graphics and Applications*, 21(5):34–41, 2001. 2
- [35] Xuqian Ren and Yifan Liu. Semantic-guided multi-mask image harmonization. In *ECCV*, 2022. 2
- [36] Xintian Shen, Jiangning Zhang, Jun Chen, Shipeng Bai, Yue Han, Yabiao Wang, Chengjie Wang, and Yong Liu. Learning global-aware kernel for image harmonization. *arXiv preprint arXiv:2305.11676*, 2023. 2

- [37] Konstantin Sofiiuk, Polina Popenova, and Anton Konushin. Foreground-aware semantic representations for image harmonization, 2020. [1](#), [2](#), [4](#), [6](#), [7](#)
- [38] Kalyan Sunkavalli, Micah K. Johnson, Wojciech Matusik, and Hanspeter Pfister. Multi-scale image harmonization. *ACM Transactions on Graphics*, 29(4):125:1–125:10, 2010. [2](#)
- [39] Yi-Hsuan Tsai, Xiaohui Shen, Zhe Lin, Kalyan Sunkavalli, Xin Lu, and Ming-Hsuan Yang. Deep image harmonization. In *CVPR*, 2017. [2](#)
- [40] Jeya Maria Jose Valanarasu, He Zhang, Jianming Zhang, Yilin Wang, Zhe Lin, Jose Echevarria, Yinglan Ma, Zijun Wei, Kalyan Sunkavalli, and Vishal M Patel. Interactive portrait harmonization. *arXiv preprint arXiv:2203.08216*, 2022. [2](#)
- [41] Aaron Van Den Oord, Oriol Vinyals, et al. Neural discrete representation learning. *NIPS*, 2017. [2](#)
- [42] Ziyu Wan, Jingbo Zhang, Dongdong Chen, and Jing Liao. High-fidelity pluralistic image completion with transformers. In *ICCV*, 2021. [2](#)
- [43] Ke Wang, Michaël Gharbi, He Zhang, Zhihao Xia, and Eli Shechtman. Semi-supervised parametric real-world image harmonization. In *CVPR*, 2023. [2](#)
- [44] Yazhou Xing, Yu Li, Xintao Wang, Ye Zhu, and Qifeng Chen. Composite photograph harmonization with complete background cues. In *ACM MM*, 2022. [2](#)
- [45] Ben Xue, Shenghui Ran, Quan Chen, Rongfei Jia, Binqiang Zhao, and Xing Tang. Dccf: Deep comprehensible color filter learning framework for high-resolution image harmonization. In *ECCV*, 2022. [1](#), [2](#)
- [46] Su Xue, Aseem Agarwala, Julie Dorsey, and Holly E. Rushmeier. Understanding and improving the realism of image composites. *ACM Transactions on Graphics*, 31(4):84:1–84:10, 2012. [2](#)
- [47] Ye Yu, Abhimitra Meka, Mohamed Elgharib, Hans-Peter Seidel, Christian Theobalt, and William AP Smith. Self-supervised outdoor scene relighting. In *ECCV*, 2020. [2](#), [3](#)
- [48] Chuanxia Zheng, Tat-Jen Cham, and Jianfei Cai. Pluralistic image completion. In *CVPR*, 2019. [2](#)
- [49] Jun-Yan Zhu, Philipp Krähenbühl, Eli Shechtman, and Alexei A. Efros. Learning a discriminative model for the perception of realism in composite images. In *ICCV*, 2015. [2](#)
- [50] Jun-Yan Zhu, Richard Zhang, Deepak Pathak, Trevor Darrell, Alexei A Efros, Oliver Wang, and Eli Shechtman. Toward multimodal image-to-image translation. *NIPS*, 2017. [2](#)